JOURNAL OF MATERIALS SCIENCE 23 (1988) 3519–3527

Crystallization embrittlement of Ni–Ti–B glasses

D. G. MORRIS, N. MERK, M. A. MORRIS
Institute of Structural Metallurgy, University of Neuchâtel, CH-2000 Neuchâtel, Switzerland

While metallic glasses have excellent toughness and ductility in the as-cast and unrelaxed state, the process of crystallization leads to a nearly continuous and significant embrittlement. This change is examined on three Ni–Ti–B glasses and related to the morphology and distribution of the crystals obtained. For the partially crystallized materials, failure still occurs after intense shear on one well-defined shear plane, and it is shown how the crystals act as stress and strain incompatibilities causing localized crack or cavity formation. The relationships between sample mechanical properties, fracture surface characteristics and crystal distributions allow an analysis of cavity nucleation and growth rates, and thereby make it possible to suggest microstructures which may maintain reasonable toughness.

1. Introduction

Metallic glasses are generally characterized by good hardness or strength, as well as significant ductility and toughness [1, 2]. Plastic deformation occurs by intense shear along well-defined shear planes oriented along the directions of maximum shear stress. During crystallization, however, these materials lose their ductility and become very brittle [3, 4]. The embrittlement occurring during crystallization is generally understood as caused by the formation of cavities where particles intersect the intense shear band [4, 5] in much the same way as for cavity nucleation during the fracture of crystalline materials containing particles [6].

Only on a few occasions, however, have these ideas been examined quantitatively. For example, Zielinksi and Ast [7] have considered the stress concentration at an obstacle at the tip of a shear band, and the applied shear stress (τ^*) necessary to open up a free surface

$$\tau^* = \left(\frac{4\gamma G}{\pi x(1-\nu)}\right)^{1/2} \quad (1)$$

where γ is the surface energy, G the shear modulus, ν Poisson's ratio, and x the length of the shear band. This approach is identical to that for the formation of cleavage cracks in steel [8, 9]. By substitution of typical values for particle dispersions in a metallic glass, they came to the conclusion that particle cracking could fairly readily be produced for many particles [7]. These arguments can in fact be extended to consider, again as has been done for cavity nucleation at particles in crystalline materials [10], that the stress concentration must be supported by a particle of finite size (ϕ) and the stress necessary to cause cavitation or cracking becomes

$$\tau = \tau^* \left(\frac{\phi}{\lambda}\right)^{1/2} \quad (2)$$

where τ^* has the value defined in [1] and λ is the pile-up length, taken as half the separation between the obstructing particles.

Argon has considered the nucleation of cavities at small particles in terms of the plastic deformation necessary to open up the free surface and to cause the cavity to reach a stable size [6, 11]. According to these arguments, cavity nucleation will be extremely difficult for small amounts of crystallinity when distributed in the form of small (less than 20–25 nm) particles. These ideas are supported by the study of Freed and Vander-Sande [4] who found that small numbers of small crystals did not lead to significant embrittlement. As such these results correspond to the stage where the ductilization phenomenon was observed in the prior report [12].

The present work examines the embrittlement occurring during the crystallization of a series of three Ni–Ti–B metallic glasses. The crystallization behaviour of these materials has previously been reported in detail [13] as well as the fracture toughness variations during crystallization [12]. In this previous study it has been shown that the toughness decreases steadily during crystallization, apart from a period of slight ductilization at the beginning of crystallization explained in terms of slip-band obstruction by the small crystals without yet the creation of significant extra failure sites. It has also been shown [12] that the fracture surface changes during crystallization, that the shear offset occurring before fracture can be related to the measured toughness value, and that the shear offset and size of dimples on the fracture surface are closely related for a given alloy.

The basic model which will be used to describe the failure of a partially crystallized material is shown schematically in Fig. 1. Shear is considered to take place on a well-defined plane, as observed experimentally. This initial consideration is certainly true for a fully glassy alloy and remains true as long as the alloy is still mainly glassy, say up to 50% or so crystallization. The intense shear causes stress and strain

0022–2461/88 $03.00 + .12

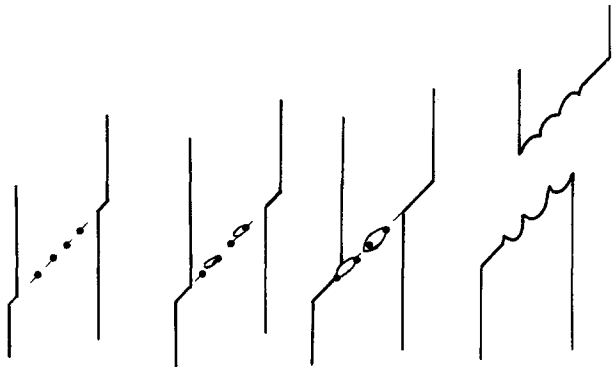

Figure 1 Illustration of the fracture model used in the present analysis. Shear along a direction of high shear stress causes cavity nucleation and growth at particles on the shear band. Failure occurs when the cavities cover essentially the entire cross-section giving rise to the characteristic shear offset and dimpled fracture surface.

concentrations at obstacles in the shear plane leading to localized cavitation or cracking. Such cracks or cavities propagate under the action of the shear deformation until they cover virtually the entire cross-section – failure has occurred. This simplistic model assumes that essentially no normal stress applies across the shear plane. In the typical fracture toughness tests the applied stress was less than one tenth of the tensile strength of the material, and therefore the simple fracture criterion seems justified.

It is important to notice that the correlation of fracture surface parameters and particle distribution makes it possible to evaluate the nucleation and growth rates of cavities (or cracks) at particles: this is illustrated with reference to Fig. 1. Consider that, at an intermediate stage of failure, the shear displacement is δ and the cavity size d. The relationship of δ to d is related to the growth behaviour of the cavity, as

$$\delta = ad^n \tag{3}$$

or, at failure, as

$$\Delta = aD^n \tag{4}$$

where Δ and D are the shear offset and dimple size measured on the fracture surface. For example, assuming that cavity growth occurs at the same rate as the shear, and that a nucleation shear (c) was necessary to form the cavity, we obtain

$$\Delta = D + c \tag{5}$$

In an analogous way, information on the nucleation kinetics will be obtained from the relationship between the final cavity size (dimple size) and the spacing between the crystalline particles (λ) (or ($\lambda - \phi$) if the particle size (ϕ) is important). In this way the relationship

$$D = m(\lambda - \phi) + p \tag{6}$$

suggests an incubation term associated with nucleation (the term p) and the likelihood of cavity formation at a given particle as $1/m$. Thus, in Fig. 1, the value of n is 2 since one-half the particles lead to cavitation.

The number of particles of size ϕ intersecting a given plane is

$$N_p = \frac{\phi}{\lambda^3} \tag{7}$$

This expression is applicable in the present case provided the shear band thickness is less than the particle size. Estimates of the shear band thickness have been given as 10–20 nm [3], while the particle sizes range from 30 nm at the point where crystallization embrittlement begins to above 200 nm. Assuming that a fraction f of particles leads to cavitation, the number of cavities per unit area is

$$N_c = f\frac{\phi}{\lambda^3} \tag{8}$$

and considering that this fraction depends inversely on the ratio ϕ/l, as suggested in Equation 2, we have

$$N_c = g\left(\frac{\lambda}{\phi}\right)\frac{\phi}{\lambda^3} = \frac{g}{\lambda^2} \tag{9}$$

The dimple size at failure would then, simply, be

$$D = N_c^{-1/2} = \lambda g^{-1/2} \tag{10}$$

It is clear from the relationships developed here that a detailed study of shear offsets, cavity (dimple) sizes and spacings of cavities and particles will be useful for learning about nucleation and growth rates during the shear and failure of partially crystallized alloys. It is clear that, ideally, these rates should be determined on a given material as different amounts of shear are accumulated and as fracture approaches. In the present work an easier approach has been taken, namely of assuming an equivalence of the nucleation and growth rates of differently heat-treated material, and examining the fracture surfaces only. This is equivalent to considering that the material-dependent terms (a, n, c, m, p, f and g in Equations 3–10) are alloy dependent but not heat-treatment dependent. While not precisely correct, this does not seem an unreasonable supposition, at least for a first analysis.

2. Experimental details

The three alloys examined were the same as those treated in the preceding paper [12], namely Ni-$B_{19.1}Ti_{2.1}$ (alloy A), Ni-$B_{18.2}Ti_{3.8}$ (alloy B) and Ni-$B_{17.9}Ti_3$ (alloy C), where details of heat treatments and mechanical testing procedure were also given. It should be recalled that alloy A crystallizes by the formation of a few, large eutectic colonies, alloy B by forming many, small τ phase crystals, and alloy C a mixture of both types. The fracture surfaces were examined, after failure, using a Cambridge 250 scanning electron microscope. In addition, shear band and crack interactions with particles were examined using transmission electron microscopy. Shear band interactions with particles were studied after slightly bending the partially crystallized material. Thin foils were then prepared from either the tensile side or the compressive side of the bent sample by blanking off one of the acid jets in a twin-jet electropolishing device and thereby electropolishing only from the opposite side. Crack interactions with particles were examined on lightly deformed thin-foil samples: a number of

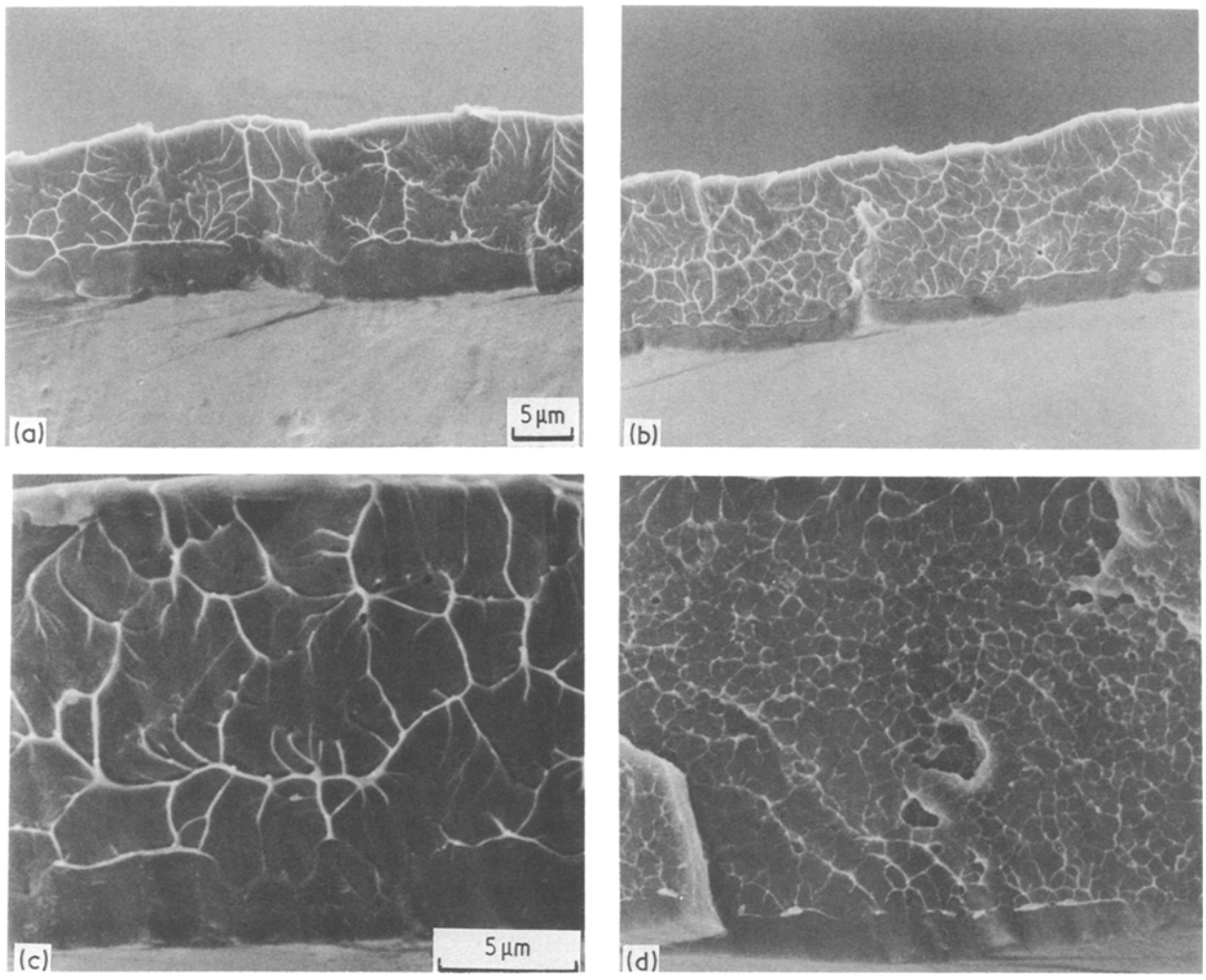

Figure 2 Scanning electron micrographs illustrating the influence of different amounts of crystallization (a)–(b) and different sizes and distributions of crystals (c)–(d) on fracture surface morphology: (a) alloy C after 2 h at 300° C, about 0.2% crystallized; (b) alloy C after 3 h at 300° C, about 1.5% crystallized; (c) alloy A after 2 min at 350° C, about 0.5% crystallized; (d) alloy B after 11 min at 350° C, about 0.5% crystallized.

cracks was always found running from the edge of the electron-transparent areas into the thicker areas of the foils.

3. Results

According to the model outlined in Fig. 1, as crystallization takes place and the sites where cavitation may occur during deformation become more numerous, as fracture toughness decreases the number of cavities or dimples on the failure surface should increase and accordingly the dimple size and failure offset decrease. This is clearly illustrated in Fig. 2. During crystallization both the amount of shear offset and the dimple size decrease (Figs 2a and b). This effect depends on the distribution of the particular particles present, as seen in Figs 2c and d, where the finer dimple size is seen to correspond to the alloy containing many small τ phase particles rather than fewer, larger eutectic particles. This relationship between cavity nucleation, dimple formation and final failure is well illustrated in Fig. 3. Many of the dimples seen are clearly associated with small cracks or cavities which may have formed because of a crystalline particle. In addition, in this figure, it is clear that the cavities have grown to cover essentially the entire surface before remaining ligaments are torn out during the final tensile stage of failure.

Quantitative relationships between the fracture surface parameters and crystal distributions are illustrated in Figs 4–6 and summarized in Table I. In

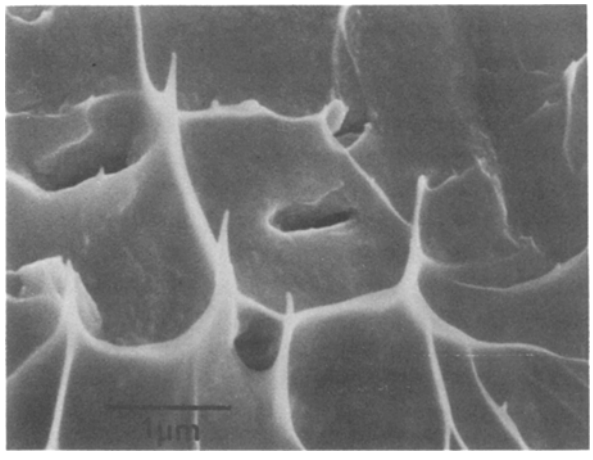

Figure 3 Fracture surface from partially crystallized sample showing that many of the dimples originated at cracked or cavitated inhomogeneities, presumably particles. During final fracture the remaining ligaments are pulled out. Alloy A afte $3\frac{1}{2}$ min at 350° C.

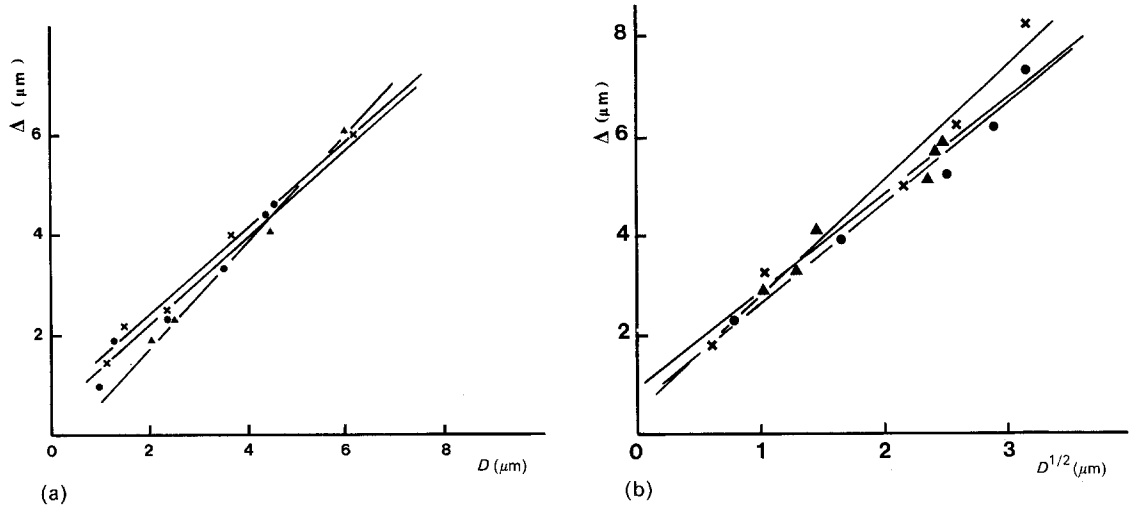

Figure 4 Relationships between shear offset at failure (Δ) and dimple size on the fracture surfaces of samples of (a) alloy A (x 350° C, ● 300° C, ▲ 280° C) and (b) alloy C (x 350° C, ● 300° C, ▲ 260° C) .

Fig. 4 it is seen that the shear offset before failure (Δ) and the average dimple size (D) are related linearly (in fact a one-to-one relationship) for the alloy A and by a parabolic relationship for alloy C: alloy B showed the same parabolic relationship as alloy C. These relationships correspond to those outlined in Equations 4 and 5, with an intercept close to zero in each case: the values of the slopes of the lines obtained at each temperature are given in Table I. Relationships between the dimple size and the distribution of crystalline particles are illustrated in Fig. 5. For alloy A, Fig. 5a, there is a linear dependence between the dimple size and the interparticle spacing, expressed as $(\lambda - \theta)$ where λ is the spacing between particles and ϕ the particle size. The slope of the line varies with temperature, as reported in Table I. For alloy B, Fig. 5b, a similar dependence is observed, but better described directly in terms of the interparticle spacing λ. Again Table I shows that the slopes of the lines are temperature dependent. It should be noted that the linear relationship between D and λ is in agreement with the relationship of Equation 10, also showing some nucleation or growth incubation effect. For alloy C two possible relationships between D and λ may be found, taking account of only the few, large eutectic particles present, or taking account of all the particles. For both a reasonable linear relationship is obtained, reported in Table I, and it is not possible to decide a preference for one relationship or the other.

From the relationships between shear offset and dimple size, and between dimple size and particle spacing, it is clear that a relationship exists between shear offset and particle spacing. This is shown in Fig. 6 for alloys A and B and the relationships are summarized in Table I for the three alloys. For the alloy C three possible relationships are indicated, one related to the large eutectic particles and two related to the many small particles (the scatter in data points prohibits a precise distinction between one or the other). Overall it can be seen that alloy C most closely resembles alloy B in its fracture behaviour, and hence it appears that the many, small τ particles present in the alloy C are more important in determining fracture than the fewer, larger eutectic particles.

Interactions between cracks formed in thin foils and the particles present are useful in giving an overall impression of the influence of these particles, even if the different stress conditions during tearing the thin foil

TABLE I Relationships observed between shear offset on fracture surface (Δ), dimple size (D) and particle spacing (λ or $\lambda - \phi$)

Alloy relation	Value of slope (a, m or b)				
	260° C	280° C	300° C	350° C	375° C
A $\Delta = aD$	–	1.05	0.86	0.9	–
$D = m(\lambda - \phi) + p$	–	6.4	2.6	1.7	–
$\Delta = b(\lambda - \phi) + d$	–	4.1	2.3	1.5	–
B $\Delta = aD^{1/2}$	–	–	2.3	2.3	3.2
$D = m(\lambda - \lambda_0)$	–	–	6	11.8	11.7
$\Delta = b\lambda^{1/2} + d$	–	–	9	14	13
C $\Delta = aD^{1/2}$	2.2	–	2.15	2.4	–
$D = m(\lambda - \phi) + p$					
(τ particles only)	13	–	16	9	–
(eutectics only)	1.3	–	3.6	2.8	–
$\Delta = b(\lambda - \phi)^{1/2} + d$					
(τ particles only)	9	–	13	9	–
(eutectics only)	2.5	–	6.6	4.3	–
$\Delta = b(\lambda)^{1/2} + d$					
(τ particles only)	12	–	20	11	–

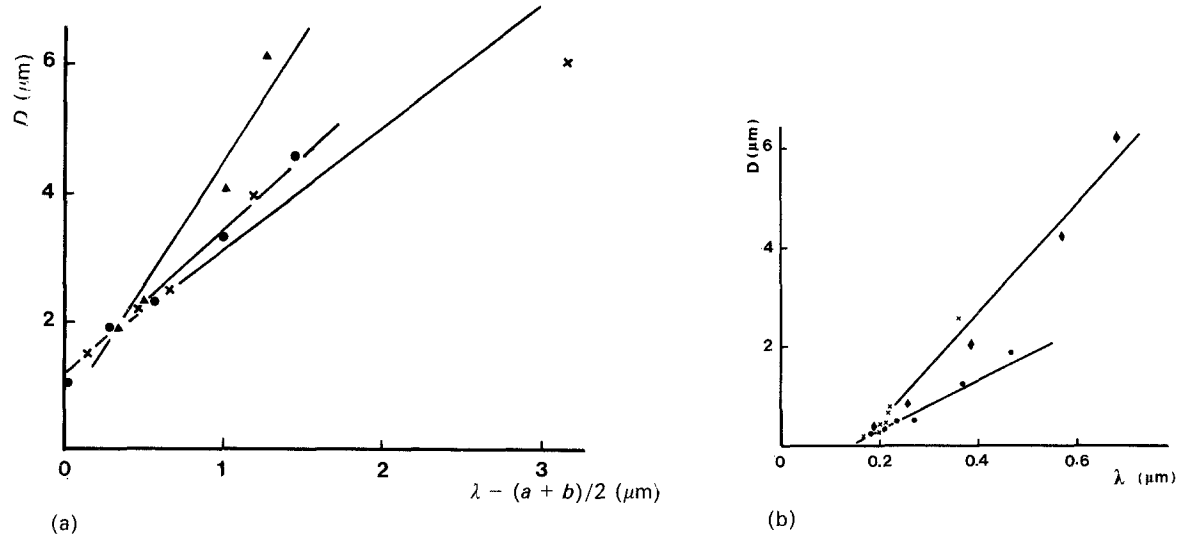

Figure 5 Relationships between dimple size on the fracture surface (D) and average spacing between particles within the material (λ). a and b are the dimensions of the elliptical eutectoid particles. (a) Alloy A and (b) alloy B. (▲ 280° C, ● 300° C, x 350° C, ◆ 375° C.)

and during fracture toughness testing the melt-spun ribbon prohibit a precise comparison. Such interactions between particles and cracks are shown in Fig. 7. In Fig. 7a it is seen that the large eutectic particles are often cracked, and often lead to a significant deviation of the crack path. It is interesting to note, however, that many of the particles do not crack, but simply deviate the propagating crack along the particle–matrix interface. As illustrated here, it is particularly those particles with their long axes perpendicular to the crack which tend most readily to crack. Fig. 7b illustrates a typical crack making its way through a glass containing many τ-phase particles. It is extremely rare, here, to find a particle which has obviously cracked or caused cavitation. More generally the crack follows the particle–matrix interface, apparently deviating around each particle encountered as the crack propagates.

Further information can be obtained from shear band interactions with particles before failure has occurred. This has been possible by studying the thin foils prepared on already deformed, partially crystalline material. Of particular interest here is an estimation of the influence of long-range stresses and interactions. For example, the increased density of the crystalline phase may cause a tensile hydrostatic field around the particle, or the cooling process following annealing may cause a compressive field because of the greater thermal dilation of the glassy matrix [7, 14]. As a result of such stress fields, Donovan [15] has reported shear bands deviating towards or away from particles before direct contact occurs. As seen in Fig. 8, there is no evidence of such long range interaction for the present alloys, neither around the large eutectic particles (A) nor around the small τ-phase particles (B). Exactly the same results were obtained on the tensile and on the compressive side of the bent samples. As such, we can correctly consider that a shear band will only interact with a particle if this lies directly in the shear plane, and the development of Equations 7–10 is supported.

Figs 9 and 10 show shear bands interacting with small crystalline particles where the beginning of cavitation is visible. In both cases it appears that cavitation has started within the particles rather than at the particle–matrix interface, although it is difficult to be

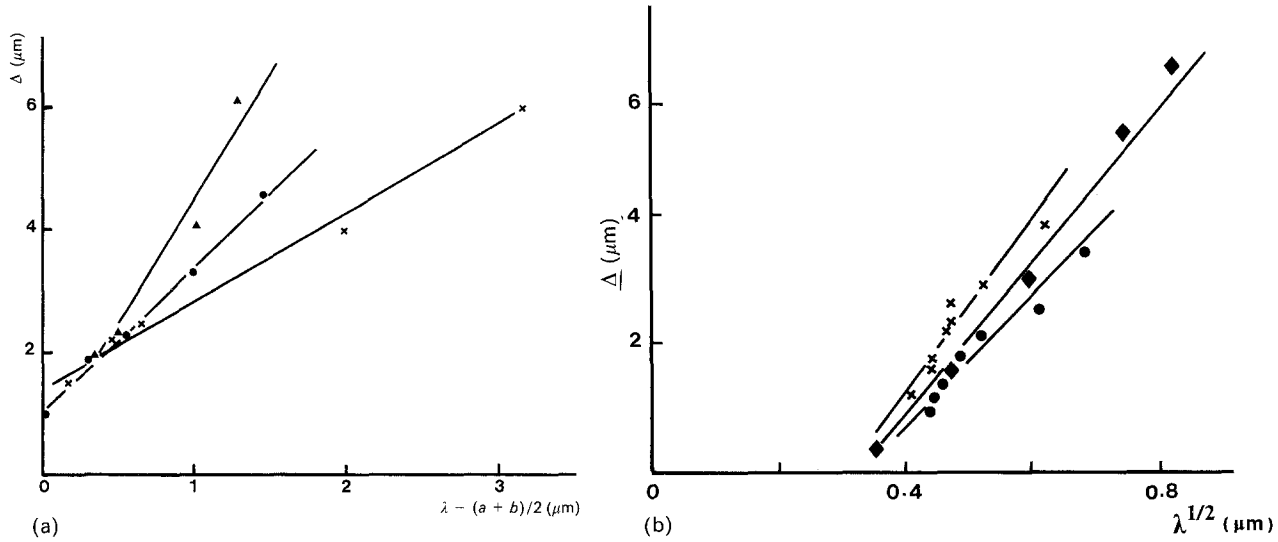

Figure 6 Relationships between fracture offset and particle spacing (λ or $\lambda - \phi$): (a) alloy A and (b) alloy B. (a and b ar the dimensions of the elliptical eutectoid particles) (▲ 280° C, ● 300° C, x 350° C, ◆ 375° C).

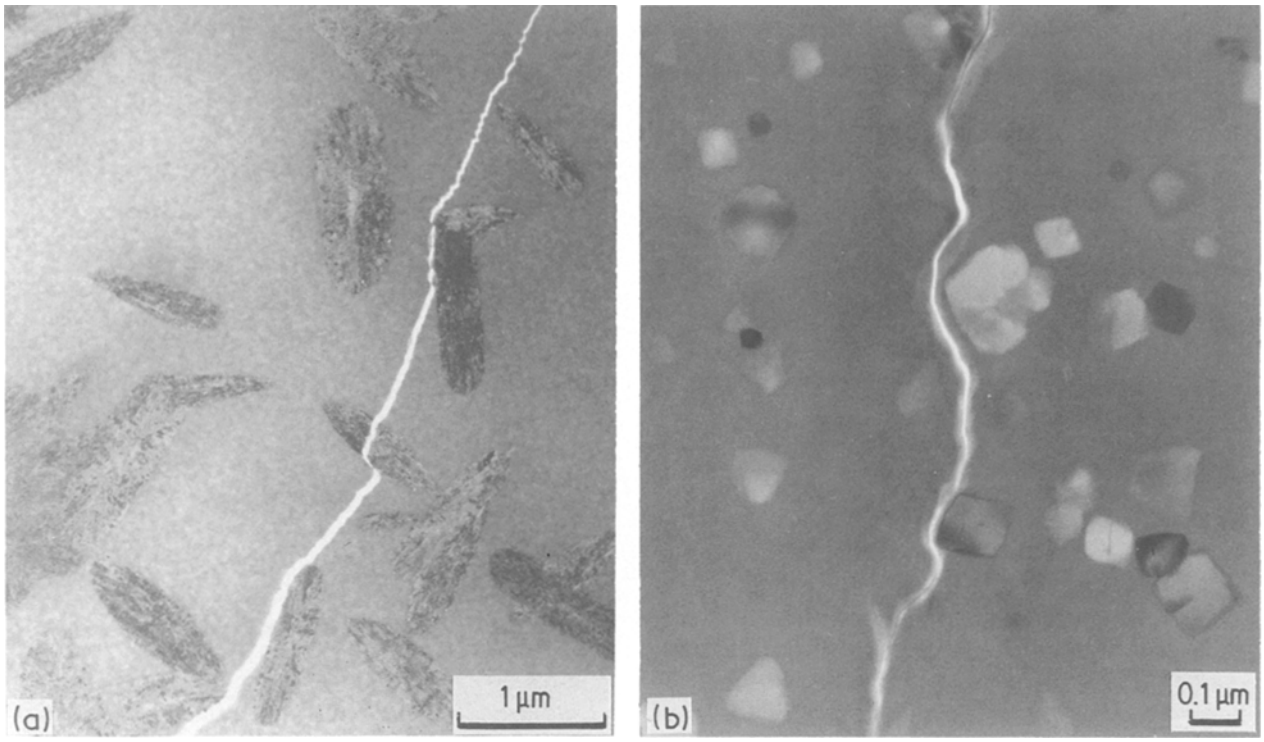

Figure 7 Cracks formed in partially crystallized thin foils (transmission electron micrographs). A few of the eutectic particles (a) are cracked, while the τ-phase particles (b) deviate the crack around the particle-matrix interface: (a) alloy A after 24 h at 280° C, (b) alloy B after 13 min at 350° C.

Figure 8 Shear bands in a slightly bent sample containing both eutectic and τ-phase crystals. Thin foil for transmission microscopy was prepared from the tensile-stress side of the bent sample. Alloy C, after 6 min at 350° C.

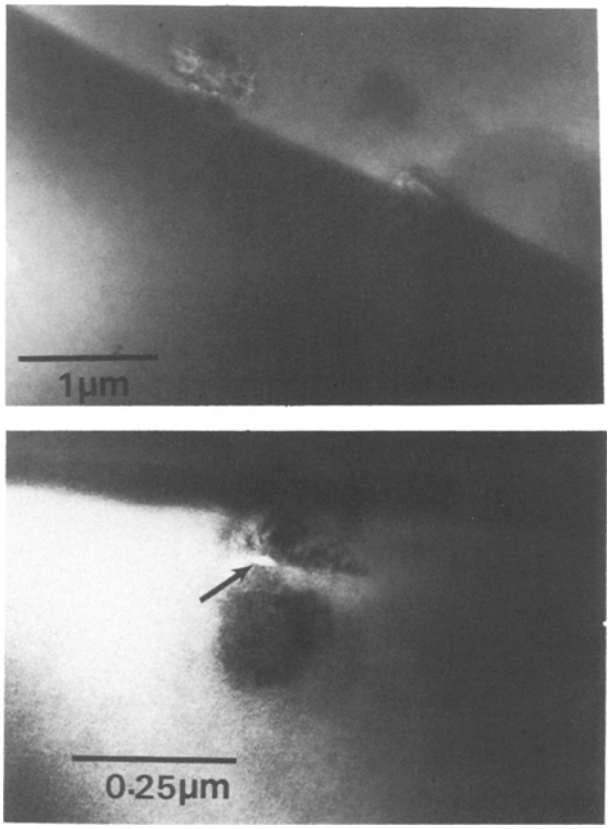

Figure 9 Shear band intersecting small eutectic particles leading to fine cavitation, apparently within the particles rather than at the particle–matrix interface.

TABLE II Estimated cavity sizes after different amounts of shear strain. (Calculated based on Equation 11, using average data from Table I)

Alloy A cavity size (μm)	Shear displacement (μm)	Alloy B cavity size (μm)
0.1	0.1	0.002
1	1	0.16
2	2	0.64
4	4	2.6
6	6	5.8

certain about this. It is, however, clear that fracture processes are initiated at the particles and thus it is the interaction of the shear band with these particles which is responsible for the embrittlement of the glass during crystallization.

4. Discussion

The fracture model outlined in Section 1 was based on crack or cavity nucleation where an intense shear band intercepted crystalline particles, followed by the shear-controlled growth of these cavities to near-complete coverage of the shear plane, and then failure in tension. It was shown how an examination of the distribution of the crystalline particles could be related to the fracture morphology to deduce information on cavity nucleation and growth. The results presented here have verified the model, and as well allowed a discussion on the cavity behaviour. Thus, it has been shown that cavity nucleation indeed takes place where the shear band meets the particle, and that only some of the particles will actually crack or cavitate. It has also been shown that the shear band is not affected by long range elastic interactions which may exist around particles, and therefore the shear band – particle intersection probability can be treated purely on geometrical grounds. Finally, fracture has been shown to occur when the cavities have grown to cover a very significant fraction of the shear plane. We shall now proceed to a quantitative evaluation of cavity nucleation and growth rates at different types of particles.

According to Equations 4 and 5, the growth dependence of cavities may be deduced from the generalized formula

$$\Delta = aD^n + c \tag{11}$$

It should be mentioned here that the growth of cavities is implicitly assumed to depend on the shear strain, that is on plastic deformation, rather than being time, or diffusion, dependent. In view of the very high strain rates occurring within the shear bands (values in excess of 10^2–$10^3\,\mathrm{sec}^{-1}$ can be deduced from the work of Neuhauser [16]) this seems a reasonable supposition. The value of c in equation 11 represents an incubation shear displacement necessary to create a growing cavity: as seen from Table I this parameter has a value of zero indicating that nucleation and growth take place already from the very start of shear. For alloy A, containing the large eutectic particles, the values of n and a are unity (see Table I) such that cavity growth occurs at exactly the same rate as the shear displacement. For alloy B, containing the small τ-phase particles (alloy C behaves in the same way as alloy B) there is a parabolic relationship between Δ and D, see Table I. This in fact means that the initial growth rate of the very small cavities, associated with the very small particles, is very slow and later accelerates to about the same rate as the large cavities associated with the large eutectic particles – this is illustrated in Table II showing the estimated cavity sizes for the two alloys A and B after different amounts of shear strain. It would seem, therefore, that cavity growth at very small sizes may be difficult, probably because of a tendency for plastic flow around a small particle and a tendency of cavity re-healing much as described by Argon for very small cavities [6], whilst for large cavities and large particles (eutectic particles) there is little tendency to rehealing and cavity growth is a direct, shear-induced tearing process.

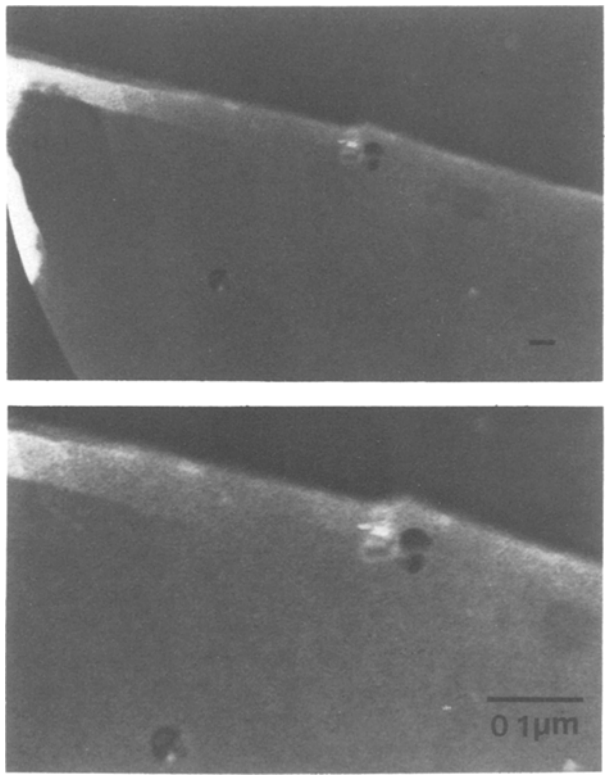

Figure 10 Shear band intersecting small particle in alloy B. The low magnification picture shows the shear band running from the edge of the foil through the particle. The higher magnification picture shows clearly the small cavity formed at the particle.

Cavity nucleation at particles may be examined in terms of Equations 6 and 10, relating the cavity size, or dimple size, to the interparticle size. It is clear here that the situation of a large particle cracking and creating already a large crack, or of a small cavity nucleating and growing slowly at a particle are two different cases, and Equation 10 may need to be modified as

$$D = (\lambda - \phi)g^{-1/2} \tag{12}$$

to consider the situation where the cavity needs only to grow over the glassy matrix between the cracked particles. The experimental data, summarized in Table I, are shown to fit these relationships (Equations 10 or 12). The relatively large scatter in the data does not

allow further discussion of a preference for one of these two relationships. Equally, the nucleation data for alloy C, which may be interpreted either in terms of the large, eutectic particles or in terms of the small, τ-phase particles, does not allow a distinction of better experimental fit to one or other data set nor a selection of the important particle species to be made. However, based on the observation of cavity growth rate for this alloy depending on the small, τ-phase particles, exactly as for alloy B, we note that cavity nucleation behaviour of alloy C can be sufficiently well interpreted in terms of these small particles.

The parameter g of Equations 9, 10 and 12 has a value of near 0.1 for alloy A and 0.01 for alloy B (also for alloy C). Accordingly, for a given alloy and heat treatment, we can say that the fraction (f) of particles which will crack or cause cavities is $0.1\lambda/\phi$ for alloy A and $0.01\lambda/\phi$ for alloys B and C (see Equations 8 and 9). During the course of crystallization the value of λ/ϕ will vary from very high, say ~ 10 at the beginning of crystallization as embrittlement begins ($\lambda/\phi \sim 10$ implies $\sim 0.1\%$ crystalline volume), to less than 2 for the heavily embrittled materials. The fraction of particles causing cavities thus varies from say 100% to 10% for the large, eutectic particles, and say 10% to 1% for the small, τ-phase particles.

These deductions would appear to be in good accord with the observations on shear bands and cracks in thin foils: only a relatively small fraction of particles encountered by a shear band actually cracks or causes a cavity to nucleate (the other particles may deviate the shear band slightly or deform with the matrix, in part dependent on the relative orientation of the shear band and the crystalline particle); the fraction of particles nucleating damage in this way is significantly larger for the eutectic particles than for the τ-phase particles (it is not known whether this is a size effect – larger particles are inherently more susceptible to crack – or may arise because of the particular phase nature or presence of interphase boundaries within the eutectic particles); finally a cracking probability dependent on λ/ϕ is exactly that expected from Equation 2.

The final relationships reported in Table I, namely those relating the shear offset and the interparticle spacing, are clearly the consequence of a given growth dependence and a given nucleation rate dependence. The relationships ($\Delta - \lambda$) may thus be regarded as important fracture criteria, relating the given microstructure (λ, ϕ) to the fracture toughness (Δ). However, no additional information on the failure process can be learned, since these relationships are clearly the products of the nucleation ($D - \lambda$) and growth ($\Delta - D$) expressions.

Finally, based on the understanding gained of failure mechanisms in partially crystalline metallic glasses, it is interesting to speculate on the best ways of limiting the embrittlement caused by the addition of crystals. This question is of particular interest in view of the development of techniques for reinforcing glasses with a cast-in dispersion of particles [17] and of controlling magnetization stresses by selective crystallization [18].

According to the present analysis, we can distinguish three parameters pertaining to the crystalline particle distribution which affect fracture: particle nature, ratio of particle size to spacing, and actual values of particle sizes and spacings. The first of these parameters depends on the degree of inherent crack resistance of the particle and the particle interface nature. The single-phase τ particles are clearly superior to the complex, eutectic phase particles in the present study. In this sense the strong TiC or WC particles used for dispersion strengthening studies (e.g. [17]) appear well chosen. The ratio of particle size to spacing (ϕ/λ) is important because it controls the stress concentration at the particles and helps determine the probability of cracking or cavitation. To limit damage this ratio should be as large as possible, hence implying a large volume fraction of crystalline material. Thirdly, the actual sizes of the particles should be large, implying a large interparticle spacing for the selected volume fraction crystalline. In this way the distance over which cavities must grow before final failure occurs will be maximized.

5. Conclusions

The fracture behaviour of partially crystalline samples has been examined based on a model of intense shear within a localized shear band causing cavity nucleation and growth where this band intercepts a crystalline particle. Failure is considered to occur under the action of relatively minor normal stresses when the cavities cover a large fraction of the shear plane.

A careful comparison of the fracture surface morphology with the distribution of the crystalline particles makes it possible to deduce the nucleation and growth rate of the cavities. The fraction of particles causing damage is relatively small, as confirmed by examination of shear bands and cracks in thin foil samples by transmission electron microscopy, and dependent on the type of particle and the ratio of size to spacing. The growth rate of the cavities also depends on the nature of the particle causing cavitation: large cavities associated with large eutectic particles grow at the same rate as the shear displacement, whilst the small cavities formed at small τ-phase particles grow initially very slowly and later at the same rate as the eutectic-cavities – the difference in cavity growth behaviour may be purely size dependent, caused by the difficulty of cavity growth at very small sizes.

The improved understanding of failure processes in these materials allows a prediction of optimum microstructure for increasing toughness by: (i) selecting particles which are strong and well bonded to the matrix (here the single phase τ particles are preferable to the eutectic phase mixture particles); (ii) selecting a large volume fraction crystallinity to limit stress concentrations at any one particle; and (iii) by selecting large particles, widely separated, such that the cavity growth distance before failure is considerable.

Acknowledgements

One of us (NM) is grateful for financial support from the Swiss Commission for the Encouragement of Research (Project No 1322) and the Swiss National

Science Foundation (Project No 2.022–0.86) during this work.

References

1. H. KIMURA and T. MASUMOTO, in "Amorphous Metallic Alloys", edited by F. E. Luborsky (Butterworths, London, 1983) p. 187.
2. L. A. DAVIES, in "Metallic Glasses" (ASM, Metals Park, Ohio, 1978) p. 191.
3. T. MASUMOTO and R. MADDIN, *Acta Metall.* **19** (1971) 725.
4. R. L. FREED and J. B. VANDERSANDE, *ibid.* **28** (1980) 103.
5. C. A. PAMPILLO, *J. Mater. Sci.* **10** (1975) 1194.
6. A. S. ARGON, J. IM and R. SAFOGLU, *Met. Trans.* **64** (1975) 825.
7. P. G. ZIELINSKI and D. G. AST, *Acta Metal.* **32** (1984) 397.
8. E. SMITH, in "Physical Basis of Yield and Fracture", Conference Proceedings Inst. Phys. Soc., Oxford (1966) p. 36.
9. E. SMITH, *Met. Sci. J.* **1** (1967) 56.
10. *Idem., ibid.* **1** (1967) 1.
11. A. S. ARGON, *J. Eng. Mater. Tech.* **98** (1976) 60.
12. N. MERK, D. G. MORRIS and M. A. MORRIS, *J. Mater. Sci.* B769.
13. N. MERK, D. G. MORRIS and P. STADELMANN, *Acta Metall.* **35** (1987) 2213.
14. G. GERARD and A. C. GILBERT, *J. Appl. Mech. (ASME)* **24** (1957) 355.
15. P. E. DONOVAN, *Mat. Res. Soc. Symp. Proc.* **28** (1984) 197.
16. H. NEUHAUSER, *Scripta Metall.* **12** (1978) 471.
17. H. KIMURA, T. MASUMOTO and D. G. AST, *Acta Metall.* **35** (1987) 1757.
18. H. R. HILZINGER and G. HERZER, *Mater. Sci. Engng* in press.

Received 22 October 1987
and accepted 17 February 1988